Available online at www.sciencedirect.com
ScienceDirect
Journal of Electron Spectroscopy and Related Phenomena 156–158 (2007) 158–163
JOURNAL OF ELECTRON SPECTROSCOPY and Related Phenomena
www.elsevier.com/locate/elspec

Experimental and theoretical study of S 2p and C 1s spectroscopy in CS_2

I.G. Eustatiu [a], T. Tyliszczak [b], G. Cooper [b], A.P. Hitchcock [b], C.C. Turci [c,*], A.B. Rocha [c], M. Barbatti [c], C.E. Bielschowsky [c]

[a] *Department of Physics and Astronomy, McMaster University, Ont. L8S 4M1, Canada*
[b] *Department of Chemistry, McMaster University, Hamilton, Ont. L8S 4M1, Canada*
[c] *Instituto de Química, Univ. Fed. do Rio de Janeiro, Rio de Janeiro, RJ 21949-900, Brazil*

Available online 5 January 2007

Abstract

Electron energy loss spectra of gas phase carbon disulfide have been recorded under dipole and strongly non-dipole conditions in the region of S 2p, and C 1s excitation. Inner-shell triplet states have also been observed by measuring near threshold C 1s energy loss spectra using a wide range of angles (4–20°) and impact energies (130–1300 eV). The optical oscillator strength (OOS) and generalized oscillator strength profiles (GOS) have been calculated for vertical excitation from the ground $X^1\Sigma_g^+$ electronic state to several C(1s) and S(2p) inner-shell electronic excited states of CS_2 molecule, using high level ab initio (HF-CI) calculations.

Keywords: CS_2; Generalized oscillator strengths; Inner-shell excitation; Triplet state; (HF-CI) calculations

1. Introduction

Inner-shell excitation can be induced either by photoabsorption or charged particle impact. In the present work, electron energy loss spectroscopy (EELS) has been used to study inner-shell excited states of carbon disulfide, CS_2.

Carbon disulfide is produced naturally by several types of soil, sediment and aquatic microorganisms, vegetation, forest and grass fires and volcanoes. Worldwide, at least 40% and possibly as much as 80% of releases are a result of natural or biogenic activity. Carbon disulfide is rapidly metabolized by organisms and does not bioconcentrate or biomagnify. As carbon disulfide is mainly released to and detected in air, this is a critical compartment in the assessment of risk to the environment and its gas phase study is very important. The experimental study of the interaction of electrons with CS_2 can be directly applied to the solar wind electrons interaction with the molecules present in comets. Therefore, the electronic structure and excited states of carbon disulfide, as well as its electronic transitions probabilities and absolute photoabsorption oscillator strengths are useful to analyze observed data from atmosphere.

Under small momentum transfer conditions electron scattering is dominated by electric dipole transitions and therefore simulates photoabsorption. Conversely, at large momentum transfer optically forbidden quadrupole and higher order electric multipole transitions can be excited [1–10]. When the incident electron energy is near the inner-shell excitation threshold, spin-exchange transitions can be excited by the exchange interaction of bound and incident electrons. Spin-forbidden inner-shell transitions have been observed in N_2 [11], CO [12,13], CO_2 [14], N_2O [15], COS, CS_2 and C_2H_2 [16].

The molecules CO_2, N_2O, COS and CS_2 are closely related triatomic linear molecules. This paper presents results for the inner-shell electron energy loss spectroscopy (ISEELS) of CS_2 molecule in the C 1s and S 2p regions. In addition to observations of quadrupole transitions, singlet–triplet transitions have been observed and used to aid spectral assignment.

The literature on the core excitation spectra of CS_2 [17–20] contains inconsistencies in both spectral shapes and interpretation. In particular the positions of the core $\rightarrow \sigma^*$ excitations are not well established. One goal of this study is to provide a consistent spectral interpretation of the core excitation spectra of CS_2.

2. Experimental

Electron energy loss spectra of CS_2 in the regions of C 1s, and S 2p excitations were acquired with a variable impact energy, variable scattering angle and electron energy loss spec-

* Corresponding author. Tel.: +55 21 2562 7001; fax: +55 21 2562 7106.
E-mail address: cassia@iq.ufrj.br (C.C. Turci).

0368-2048/$ – see front matter © 2007 Elsevier B.V. All rights reserved.
doi:10.1016/j.elspec.2006.12.065

trometer. A detailed description of the apparatus, its operating procedures and data analysis methods has been published elsewhere [1,3]. Freeze–pump–thaw iterations were performed on CS_2 (stated boiling point range of 46.1–46.6 °C), which was otherwise used as received from the commercial supplier (Aldrich, 99.9% purity). The pressure of the differentially pumped region connected to the gas cell was 5×10^{-6} torr during data acquisition. The energy scales of all spectra were calibrated internally using previously published assignments [21].

3. Theory

We have calculated the optical (OOS) and generalized oscillator strength (GOS) for the vertical excitation from the ground $X^1\Sigma_g^+$ electronic state to several C 1s and S 2p inner-shell electronic excited states of CS_2 molecule. The electronic wave functions for the ground and C 1s excited states were determined with the configuration interaction (CI) method expanded on a C: (12s, 6p, 1d)/[10s, 4p, 1d] and S: (15s, 9p, 1d)/[11s,5p, 1d] Gaussian basis sets. The employed Gaussian basis sets for the C and S atoms were chosen bearing in mind a good description of: (1) the core molecular orbitals and (2) the external single occupied orbital after excitation of one electron from the core. Hence, we have used very uncompressed basis sets with several basis functions for the core region and several diffuse functions for the external region.

The molecular geometry has been determined using the above described basis set at second-order Møller–Plesset level of theory presenting the $D_{\infty h}$ point group with 1.538 Å as the CS-distance. The occupied and improved virtual orbitals (IVO) were determined independently for the ground and each excited state and, as a consequence, they are not orthogonal. This means that the molecular basis for the CI calculation was optimized for each molecular state and includes, for the excited states, the strong relaxation that takes place in the formation of an inner-shell excited state.

Configuration interaction calculations were performed for each molecular state, allowing single and double excitations (SDCI) for the reference configuration to a virtual space composed of 25 virtual orbitals ($6\sigma_g^+$, $6\pi_g$, $1\sigma_g^-$, $5\sigma_u^+$, $6\pi_u$, $1\sigma_u^-$). In each state, the SDCI calculation was performed for about 6000 configurations.

The second-order CI does not balance adequately the fundamental and excited states. This produces errors in the transition energies of about 2 eV. The fourth-order excitations in the CI eliminate these deviations [22]. In our case, computational limitations did not allow to extend the calculation to SDTQ CI level. However, we note that although the absolute values of transition energies were not in good agreement with experimental ones, the relative values show a good agreement, as may be seen in Table 1.

For the excitation from the S 2p orbitals, generalized multistructural (GMS) wave functions [23,24] were used in order to take into account core hole localization effects without breaking the full molecular symmetry. The GMS wave function is defined as

$$\Psi_{GMS} = \sum_{l=1}^{N_{STRUCT}} \sum_{i=1}^{N_{SEF}} c_i^l \Phi_i^l, \quad (1)$$

Table 1
Energies, line shapes, widths and assignments of features of the C 1s spectra of CS_2

Peak	Energy (eV)			Term value	Line type[a] (width)	Assignment	
	This work (experiment)	This work (theory)	Literature				
1	285.2[b]	286.6 (285.0)[c]	285.2[d]	7.9	*G* (0.85)	$3\pi_u^*(^3\Pi)$	$[3\pi_u]$[e]
2	286.1	287.7 (286.1)	286.1[f]	7.0	*G* (0.70)	$3\pi_u^*(^1\Pi)$	$[3\pi_u]$
3	289.4	291.2 (289.6)	288.9[d]	3.7		$3s\sigma_g^*(^3\Sigma_g)$[d]	$[7\sigma_g^+]$
4	289.5	291.3 (289.7)	289.6[d]	3.6	*G* (0.91)	$3s\sigma_g^*(^1\Sigma_g)$	$[7\sigma_g^+]$
5	290.7	292.3 (290.7)	290.6[d]	2.4	*G* (1.25)	$3p\sigma_u$	$[6\sigma_u^+]$
		295.4 (290.9)				$3p\pi_u$	$[4\pi_u]$
6	292.4	296.6 (292.1)	292.4[d]	0.7	*G* (1.46)	$7\sigma_g^*(^1\Sigma_g)$	$[8\sigma_g^+]$
		294.1 (292.4)					$[3\pi_g]$
		294.2 (292.6)	293.1[g]		*E* (5.23)	IP	
7	293.3	298.0 (293.5)	293.4[d]	−0.2	*G* (0.93)	$6\sigma_u^*$	$[7\sigma_u^+]$
8	295.8		295.8[d]	−2.7	*G* (0.78)	$2e^-$	
			297.3[d]			$2e^-$	
9	299.6		299.4[h]	−6.3	*G* (2.53)	$2e^-$	

[a] *G* is the Gaussian profile and *E* the error function edge shape.
[b] Value obtained from fitting for the spectrum acquired with final energy of 130 eV above threshold at 4°.
[c] The values in parentheses are E_{theo} multiplied by a normalization factor *f*. For the first CI root in each symmetry, *f* = 286.1/287.7 and for the second CI roots, *f* = 292.1/296.6.
[d] Ref. [16].
[e] In the square brackets are shown the theoretical molecular orbital for which one electron from the C $1s2\sigma_g^+$ orbital was promoted.
[f] All energies were established by calibrating the C $1s \rightarrow 3\pi_u^*$ transition to this value [20].
[g] Ref. [27].
[h] Ref. [20].

where Φ_i^l represents the ith spin-adapted eingenfunction (SEF) of the lth bonding structure and c_i^l its weight in the expansion shown in Eq. (1) and is calculated variationally. Each Φ_i^l is a Hartree–Fock or a CI wave function. We have considered the following three structures ($N_{STRUCT} = 3$ in Eq. (1)) for each excited state:

Structure 1 is a Hartree–Fock wave function with molecular orbitals optimized in the presence of a 2p hole localized upon the first sulphur atom.
Structure 2 is a Hartree–Fock wave function with molecular orbitals optimized in the presence of a 2p hole localized upon the second sulphur atom.
Structure 3 is a SDCI wave function (SD is the single and double) with molecular occupied and virtual orbitals optimized in the presence of a 2p delocalised hole.

This approach considers relaxation, valence correlation and localization effects and retains the full molecular symmetry. The wave functions for the ground (CI) and excited states (CI or GMS), in spite of being a suitable description for the states involved in the transition, have the disadvantage of being mutually nonorthogonal. This requires considerable computational effort for calculating the transition matrix elements. The matrix elements for the scattering amplitude between the nonorthogonal wave functions were calculated using a bi-orthogonalization procedure [25]. For this purpose, unitary transformations are applied to the two sets of N non-orthogonal molecular orbitals, turning $(N-1)$ of them orthogonal.

4. Results and discussion

4.1. Spectroscopy of CS_2

Carbon disulfide, a linear, 16 valence electron system isoelectronic with CO_2, N_2O and COS, is a molecule of astrophysical and astronomic interest [26]. Its ground state electronic configuration, represented by the term $X^1\Sigma_g^+$, is:

Core orbitals

$$(1\sigma_u^+)^2(1\sigma_g^+)^2 \quad (2\sigma_g^+)^2 \quad (2\sigma_u^+)^2(3\sigma_g^+)^2 \quad (3\sigma_u^+)^2(4\sigma_g^+)^2(1\pi_u)^4(1\pi_g)^4$$
$$\cdots S\ 1s\cdots \qquad C\ 1s \qquad \cdots S\ 2s\cdots \qquad \cdots\cdots S\ 2p\cdots\cdots$$

Valence orbitals

$$(5\sigma_g^+)^2(4\sigma_u^+)^2(6\sigma_g^+)^2(5\sigma_u^+)^2(2\pi_u)^4(2\pi_g)^4$$

Virtual orbitals

$$(3\pi_u)^0(7\sigma_g^+)^0(6\sigma_u^+)^0(4\pi_u)^0(8\sigma_g^+)^0(3\pi_g)^0(7\sigma_u^+)^0$$

Within a minimal basis set, an LCAO-MO description predicts the existence of four vacant molecular orbitals, two of which are degenerate with π_u symmetry, while the other two have σ_g and σ_u symmetry. The lowest energy unoccupied orbitals are thus expected to be $3\pi_u$, $7\sigma_g$ and $6\sigma_u$ analogous to the $2\pi_u$, $5\sigma_g$ and $4\sigma_u$ of CO_2, respectively [1].

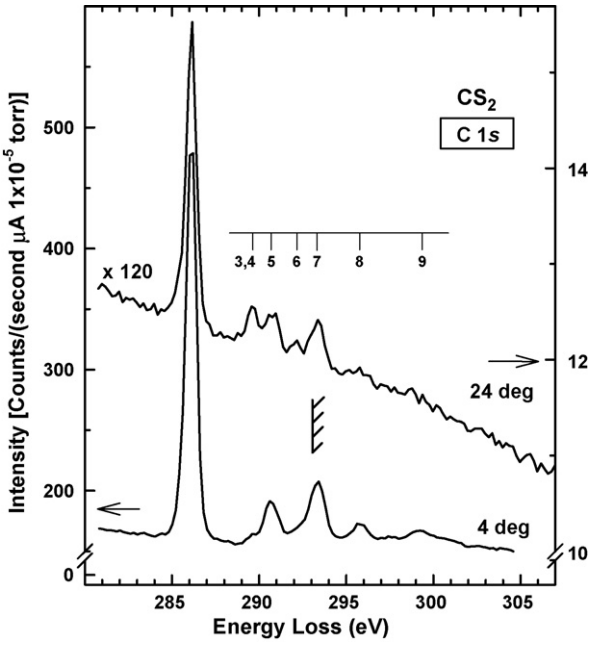

Fig. 1. Comparison of C 1s energy loss spectra of CS_2 recorded at final electron energy of 1300 eV at 4° ($K^2 = 1.57$ a.u.$^{-2}$) and 24° ($K^2 = 19.7$ a.u.$^{-2}$). The data has been normalized to gas pressure, incident beam current and acquisition time. Note the 120-fold scale factor between the 4° and 24° data. The hatched line indicates the C 1s IP as determined by X-ray photoelectron spectroscopy [27].

4.1.1. C 1s spectroscopy

Fig. 1 presents the C 1s spectra of CS_2 recorded under small ($\theta = 4°$, $K^2 = 1.57$ a.u.$^{-2}$) and large ($\theta = 24°$, $K^2 = 19.7$ a.u.$^{-2}$) momentum transfer conditions. The spectra were recorded with a final electron energy of 1300 eV. The general features are in agreement with literature [16,20]. The spectra plotted have been normalized to the beam current, pressure and time, but they have not been subjected to the geometric or kinematic corrections. The spectra were calibrated using the energy of 286.1 eV for the C 1s $\rightarrow 3\pi_u^*(^1\Pi_u)$ state reported by Millie et al. [28]. Table 1 summarizes the energies of the C 1s spectral features derived from the constrained multiple file curve-fit analysis.

At both angles, the spectrum is dominated by the intense feature at 286.1 eV, here called peak 2 (peak 1 is associated with a triplet state—see below). However, there is a dramatic fall-off in intensity as the scattering angle increases—the as-recorded 24° spectrum is about 120-fold weaker than that at 4°. This is partly due to the rapid decrease of the excitation cross section with increasing angle, but it also reflects reduced overlap of the incident electron beam and analyzer acceptance cone [3]. The dominant peak is the $X^1\Sigma_g^+ \rightarrow {}^1\Pi_u(C\ 1s2\sigma_g^{-1},\ 3\pi_u^*)$ transition, analogous to the first discrete peak in the C 1s spectrum of CO_2 [1].

Fig. 2 shows an expanded presentation of the discrete region of C 1s spectra of CS_2 acquired with better resolution than the spectra displayed in Fig. 1. The final energies are 1300 and 130 eV above threshold at 4°, 130 eV above threshold at 20° and 1300 eV above threshold at 24°. These values were chosen to selectively enhance specific classes of transitions. Thus, the (130 eV, 20°) condition highlights triplet states associated with both dipole and quadrupole allowed transitions

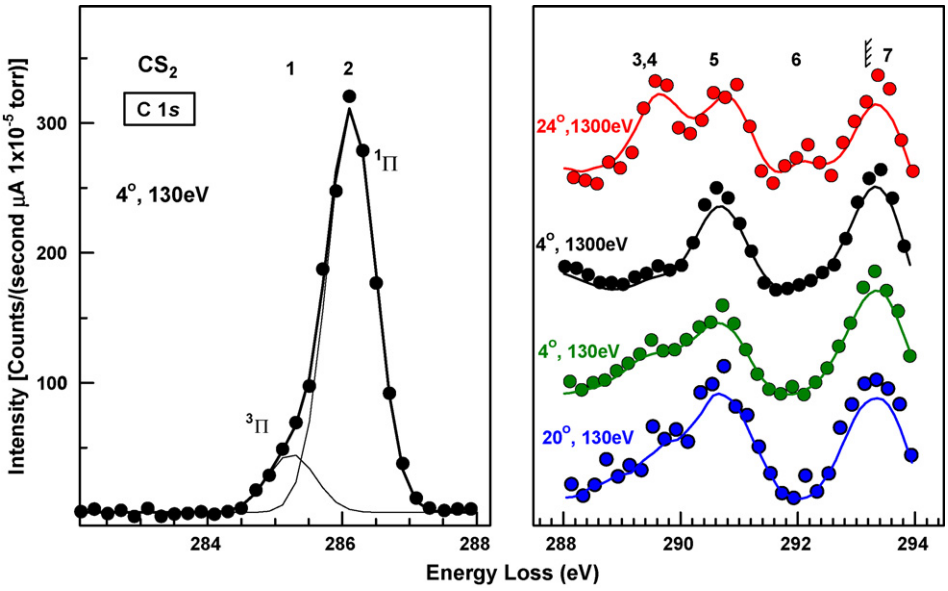

Fig. 2. *Left*: Electron energy loss spectra of CS_2 in the region of the (C $1s^{-1}$, π^*) $^3\Pi$ and $^1\Pi$ states recorded at scattering angle 4° and 130 eV final energy. *Right*: Detail of the 288–294 eV energy loss recorded under a variety of scattering angles and impact energy conditions.

to valence-like final states. At (130 eV, 4°) just the triplet states associated with dipole allowed transitions are expected. Indeed, on the low energy side of the peak 2, there is another peak (peak 1) at an energy of 285.2 eV, previously reported and assigned to the triplet state associated with the C 1s → $3\pi_u^*(^3\Pi_u)$ configuration by Harrison and King [16]. The energy splitting between the singlet and triplet final states is 0.9 eV, in agreement with [16] and also with the theoretical result of 0.8 eV at HF level and 1.1 eV at SDCI level (this work). At (1300 eV, 4°) the spectrum should be dominated by the electric dipole transitions alone. Finally, at (1300 eV, 24°) the experimental conditions are favourable for quadrupole transitions to appear.

As noted in the introduction, the spectroscopic challenge is the identification of the C 1s → σ^* transitions. In the initial analysis, Wight and Brion [20] did not propose any σ^* assignments, but rather attributed the non-π^* features to Rydberg states or left them unassigned. Nenner et al. [19] proposed assignment of the dipole forbidden the C 1s → $7\sigma_g^*$ transition to a very weak feature first observed by Wight and Brion at 289.6 eV [20]. This feature corresponds to that labelled (3, 4) in the present work. On examining the small angle and large angle, large impact energy spectra in Fig. 2, features (3, 4) at 289.5 eV and feature 6 at 292.4 eV increase in relative intensity at large scattering angles, a typical signature of a quadrupole transition. There are two candidate states one might consider for these features, one is the C 1s → $7\sigma_g^*$ transition, the other is the C 1s → $3s\sigma_g^*$ transition. The 292.4 eV is too high in energy to be the $3s\sigma_g$ state. Thus, we propose that the 289.5 eV peak is the $3s\sigma_g$ ($^1\Sigma_g^+$) Rydberg state and assign the 292.4 eV peak to the C 1s → $7\sigma_g^*$ state. The assignment of the 289.5 eV peak as a Rydberg transition is consistent with the theoretical results. The main CI-determinant contributing for the final state description has a single occupation in the $7\sigma_g^+$ molecular orbital (MO), which has atomic features, just like expected for a Rydberg one. In the case of the 292.4 eV peak, the main CI-determinant has a single occupation in the $8\sigma_g^+$ MO, which has the antibonding feature expected by the proposed assignment.

Considerable intensity is also observed in the near threshold spectra (130 eV, 4°) and (130 eV, 20°). Although at the limits of our statistics, the centroid of the (3, 4) peak in the lower impact energy spectra seems to be slightly lower than in the higher impact spectra. We suggest that there is also a contribution from a C 1s → $3s\sigma_g^*(^3\Sigma_g^+)$ state. If so, the singlet–triplet splitting is small, indicative of a low degree of C 1s → $3s\sigma^*$ overlap, as expected for a Rydberg transition. Also, if the very weak 292.4 eV peak is the $7\sigma_g^*$ state, this parallels the extreme weakness of its counterpart in CO_2 [1]. Although, as a valence-type state, it would be expected to have a larger singlet–triplet splitting, the weakness probably means we would not see the triplet counterpart in the present set of measurements. The theoretical results corroborates this analysis, providing a splitting of only 0.1 eV.

Either one of the prominent features at 290.7 eV (peak 5) and 293.3 eV (peak 7) could be candidates for the dipole allowed C 1s → $6\sigma_u^*$ transition. The 290.7 eV peak is at the expected position for the dipole allowed $3p\sigma_u$ Rydberg transition, which are frequently quite intense. Thus, we attribute the 290.7 eV to the (C $1s^{-1}$, $3p\sigma_u$) Rydberg state and the 293.3 eV peak to the C 1s → $6\sigma_u^*$ state. One must also consider the possibility of Rydberg valence mixing [29–31].

The features at 295.8 eV (peak 8) and 299.6 eV (peak 9) (see Fig. 1) are assigned to multi-electron excitations. More specifically, these two resonances, together with another one at ~297.3 eV [29] that we do not resolve, are formed by transitions to the π^* state associated with the shake-up of the outer valence electrons ($2\pi_g$, $2\pi_u$, $5\sigma_u$ and $6\sigma_g$) to closely lying antibonding levels ($3\pi_g$, $3\pi_u$, $6\sigma_u$ and $7\sigma_g$) [29].

4.1.2. S 2p Spectroscopy

Fig. 3 presents the S 2p energy loss spectra of carbon disulfide recorded under dipole ($\theta = 4^\circ$, $K^2 = 0.85$ a.u.$^{-2}$) and non-dipole ($\theta = 20^\circ$, $K^2 = 13$ a.u.$^{-2}$) conditions. The spectra have been normalized to the beam current, pressure and time, and background subtracted, but they have not been subjected to the geometric or kinematic corrections. Table 2 summarizes the energies of the S 2p spectral features derived from the constrained multiple file curve-fit analysis.

The lowest energy discrete peaks observed at 163.1 eV (peak 1) and 164.2 eV (peak 2) in the S 2p spectrum are associated with the promotion of the sulphur 2p electrons to the vacant $3\pi_u^*$ valence molecular orbital. The distance between them (~1.1 eV) corresponds to the S 2p spin-orbit splitting (~1.2 eV [27]). The intensity of these two features increases at higher scattering angle, suggesting there may be a mix of states, including one or more of quadrupole character, and not a single dipole allowed transition. Because CS_2 belongs to the $D_{\infty h}$ point group and the S 2p orbitals are of symmetry π_u, π_g, σ_u and σ_g, there could be a strong non-dipole contribution from the transitions type $\pi_u \rightarrow 3\pi_u$ and $\sigma_u \rightarrow 3\pi_u$ that increases the intensity of these peaks over that of the dipole allowed $\pi_g \rightarrow 3\pi_u$ and $\sigma_g \rightarrow 3\pi_u$ transitions.

The feature located at 165.9 eV (peak 3) is assigned to the $2p_{1/2} \rightarrow 7\sigma_g^*$ transition. The S $2p_{1/2} \rightarrow 7\sigma_g^*$ transition should then appear around 167 eV, as suggested by Karawajczyk et al.

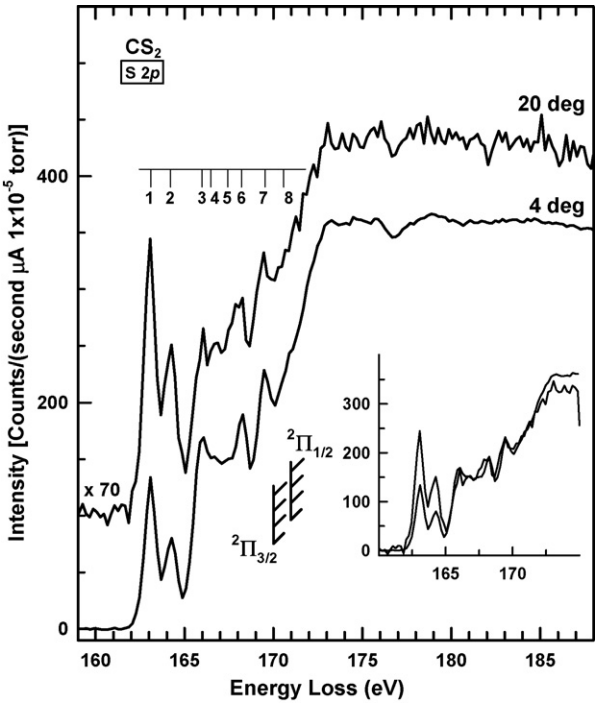

Fig. 3. Comparison of S 2p energy loss spectra of CS_2 recorded with final electron energy of 1300 eV at 4° ($K^2 = 0.85$ a.u.$^{-2}$) and 20° ($K^2 = 13$ a.u.$^{-2}$) conditions. Note the 70-fold scale factor between the 4° and 20° data. See caption of Fig. 1 for details.

Table 2
Energies, line shapes, widths and assignments of features of the S 2p spectra of CS_2

Peak	Energy (eV)		Term value				Assignment	
	This work	Literature	$T_{3/2}$	$T_{1/2}$	Line type[a]	Width	$2p_{3/2}$	$2p_{1/2}$
1	163.1	163.1[b]	6.7		*G*	0.78	$3\pi_u^*$[c]	
2	164.2	164.2[d]		6.8	*G*	0.78		$3\pi_u^*$[c]
3	165.9	165.9[d]	3.9		*G*	1.04	$7\sigma_g^*$[c]	
4	166.6	166.5[d]		4.4	*G*	0.90	$4s\sigma_g$[c]	
		167.0[c]						$7\sigma_g^*$[c]
5	167.5	167.4[d]	2.3		*G*	1.08	$4p\pi_u$[c]/$4p\sigma_u$[c]	
		167.6[c]						$4s\sigma_g$[c]
		167.8[c]					$3d\sigma_g$[c]	
6	168.3	168.2[d]	1.5		*G*	0.61	$3d\pi_g$[c]/$3d\delta_g$[e]/$5s\sigma_g$[c]/$5p\pi_u$[c]/$3d\delta_g$[c]	
		168.5[c]					$5p\sigma_u$[c]	$4p\pi_u$[c]
		168.7[c]						$4p\sigma_u$[c]
		169.0[c]						$3d\sigma_g$[c]
		169.1[c]						$3d\pi_g$[c]
7	169.5	169.5[d]		1.5	*G*	1.64		$5s\sigma_g$[c]/$3d\delta_g$[c]/$5p\sigma_u$[c]
		169.8[f]			*E*	1.25	$IP_{3/2}$	
		169.9[c]						$4d\pi_g$[c]
8	170.8	170.8[d]		0.2	*G*	0.53		$4d\delta_g$[e]
		171.0[f]			*E*	1.25		$IP_{1/2}$
		177.1[d]	−7.3	−6.1			σ_u^*[g]	

[a] *G* is the Gaussian profile and *E* the error function edge shape.
[b] All energies were established by calibrating the S $2p_{3/2} \rightarrow 3\pi_u^*$ transition to this value [20].
[c] Ref. [25].
[d] Ref. [20].
[e] Ref. [28].
[f] Ref. [27].
[g] Ref. [19].

[29], assuming similar separation of the $\pi^*_{1/2}$ and $\sigma^*_{1/2}$, and the $\pi^*_{3/2}$ and $\sigma^*_{3/2}$ states.

The line at 166.6 eV (peak 4) is assigned to the $4s\sigma_g$ Rydberg state, while the feature at 167.5 eV (peak 5) is associated with transitions into lower Rydberg orbitals of p symmetry, split into π_u and σ_u, components that we cannot resolve. The structure at 168.3 eV (peak 6) corresponds to 3d-Rydberg states from S $2p_{3/2}$, split into components $3d\sigma_g$, $3d\pi_g$ and $3d\delta_g$, which again, our spectrometer cannot resolve and a series of 5s- and 5p-Rydberg states [29]. The feature at 169.5 eV (peak 7) that we observe, is assigned by Karawajczyk et al. [29] to a series of Rydberg transitions (3d-, 5s- and 5p-) from S $2s_{1/2}$, while the 4d-Rydberg transition from S $2s_{1/2}$ is located at 170.8 eV (peak 8). The location of the σ^*_u is most likely further away in the continuum, around 177.1 eV [19].

5. Summary

Energy loss spectra of CS_2 have been recorded under dipole and strongly non-dipole conditions in the region of S 2p and C 1s excitation. The results were compared to theory and the assignments are generally in good agreement.

Acknowledgements

This research is supported financially by NSERC (Canada), the Canada Research Chair program, CNPq, FAPERJ and FUJB (Brazil).

References

[1] I.G. Eustatiu, T. Tyliszczak, A.P. Hitchcock, C.C. Turci, A.B. Rocha, C.E. Bielschowsky, Phys. Rev. A 61 (2000) 042505.
[2] A.P. Hitchcock, Phys. Scripta T 31 (1990) 159.
[3] I.G. Eustatiu, J.T. Francis, T. Tyliszczak, C.C. Turci, A.L.D. Kilcoyne, A.P. Hitchcock, Chem. Phys. 257 (2000) 235.
[4] J.S. Lee, T.C. Wong, R.A. Bonham, J. Chem. Phys. 63 (1975) 1643.
[5] J.S. Lee, J. Chem. Phys. 67 (1977) 3998.
[6] A.C.A. de Souza, G.G.B. de Souza, Phys. Rev. A 38 (1988) 4488.
[7] K.N. Klump, E.N. Lassettre, Chem. Phys. Lett. 51 (1977) 99.
[8] K.N. Klump, E.N. Lassettre, J. Chem. Phys. 68 (1978) 3511.
[9] J.F. Ying, C.P. Mathers, K.T. Leung, H.P. Pritchard, C. Winstead, V. McKoy, Chem. Phys. Lett. 212 (1993) 289.
[10] C.C. Turci, J.T. Francis, T. Tyliszczak, G.G.B. de Souza, A.P. Hitchcock, Phys. Rev. A 52 (1995) 4678.
[11] D.A. Shaw, G.C. King, F.H. Read, D. Cvejanovic, J. Phys. B 15 (1982) 1785.
[12] D.A. Shaw, G.C. King, D. Cvejanovic, F.H. Read, J. Phys. B 17 (1984) 2091.
[13] J.T. Francis, N. Kosugi, A.P. Hitchcock, J. Chem. Phys. 101 (1994) 10429.
[14] D.A. Shaw, G.C. King, F.H. Read, Chem. Phys. Lett. 129 (1986) 17.
[15] L. Ungier, T.D. Thomas, Chem. Phys. Lett. 96 (1983) 247.
[16] I. Harrison, G.C. King, J. Electron Spectrosc. 43 (1987) 155.
[17] R.G. Hayes, J. Chem. Phys. 86 (1987) 1683.
[18] R.C.C. Perera, E. Lavilla, J. Chem. Phys. 81 (1984) 3375.
[19] I. Nenner, M.J. Hubin-Franskin, J. Delwiche, P. Morin, S. Bodeur, J. Mol. Struct. 173 (1988) 269.
[20] G.R. Wight, C.E. Brion, J. Electron Spectrosc. 4 (1974) 335.
[21] A.P. Hitchcock, D.C. Mancini, J. Electro Spectrosc. 67 (1994) 1.
[22] G.G.B. de Souza, M.L.M. Rocco, H.M. Boechat-Roberty, C.A. Lucas, I. Borges Jr., E. Hollauer, J. Phys. B: At. Mol. Opt. Phys. 34 (2001) 1005.
[23] M.P. de Miranda, C.E. Bielschowsky, J. Mol. Struct. (Theochem.) 282 (1993) 71.
[24] R.E. Farren, J.A. Sheehey, P.W. Langhoff, Chem. Phys. Lett. 177 (1991) 307.
[25] C.E. Bielschowsky, M.A.C. Nascimento, E. Hollauer, Phys. Rev. A 45 (1992) 7942.
[26] R.D. Hudson, Rev. Geophys. and Space Phys. 9 (1971) 305.
[27] (a) K.H. Sze, C.E. Brion, Chem. Phys. 140 (1990) 439;
(b) C.J. Allan, U. Gelius, D.A. Allison, G. Johansson, H. Siegbahn, K. Siegbahn, J. Electron Spectrosc. Relat. Phenom. 1 (1972/1973) 131.
[28] P. Millie, A.P. Hitchcock, S. Bodeur, I. Nenner, unpublished.
[29] A. Karawajczyk, P. Erman, P. Hatherly, E. Rachlew, M. Stankiewicz, Y. Yoshiki Franzén, Phys. Rev. A 58 (1998) 314.
[30] K.H. Sze, C.E. Brion, M. Tronc, S. Bodeur, A.P. Hitchcock, Chem. Phys. 121 (1988) 279.
[31] A.P. Hitchcock, J.A. Horsley, J. Stöhr, J. Chem. Phys. 85 (1986) 4835.